

# Wavelet analysis reveals dynamic coherence between $\text{Ca}^{2+}$ waves and membrane potential oscillations in subepicardial cardiomyocytes

Danila Bobkov<sup>1,\*</sup>, Galina Sakuta<sup>8</sup>, Ekaterina Baidyuk<sup>3</sup>, Andrei Stepanov<sup>4</sup>, Igor Kubasov<sup>5</sup>, Maxim Dobretsov<sup>6</sup>, Vladimir Polyanskiy<sup>7</sup>, and Sandor Gyurke<sup>8</sup>

<sup>1,2,3</sup>Institute of Cytology of the Russian Academy of Science, 194064 Tikhoretsky ave. 4, St-Petersburg, Russia

<sup>4,5,6</sup>Sechenov Institute of Evolutionary Physiology and Biochemistry of the Russian Academy of Science, 194223 Russia

Saint-Petersburg pr.Torez 44

<sup>7</sup>Institute for Problems in Mechanical Engineering Russian Academy of Sciences (IPME RAS) St.Petersburg, Russia

<sup>8</sup>Dorothy M. Davis Heart and Lung Research Institute, College of Medicine, Ohio State University, Columbus, OH, United States

\*Correspondence: dan.bobkov@gmail.com

## ABSTRACT

$\text{Ca}^{2+}$  ions play a key role in the electrical and mechanical responses of the heart. In ischemic myocardium, calcium waves are considered as an arrhythmogenic substrate. With a deficiency of ATP caused by hypoxia, cardiomyocytes are damaged, with the formation of necrotic striation. This study examines the changes in  $\text{Ca}^{2+}$  oscillations frequencies which arose in response to ischemia in a model of isolated perfused rat heart. Sporadic  $\text{Ca}^{2+}$  waves was observed using confocal laser microscopy simultaneously with membrane potential waves in the subepicardial layers of the myocardium of an isolated rat heart under hypoxic conditions. Such waves propagate a short distance around their source and interfere with sinus rhythm. We identified high-frequency  $\text{Ca}^{2+}$  oscillators, that arise in cardiomyocytes at the sites of local damage caused by hypercontraction. The source of these waves are local  $\text{Ca}^{2+}$  release regions, associated with hypercontraction damage sites. High-frequency oscillations are non stationary in their nature, and temporal understanding is dynamics of their spectral characteristics is of great interest. In this study, we provide an approach for investigation the spatio-temporal frequency domains in multicellular specimen. Analysis of the frequency and amplitude characteristics of calcium waves in made it possible to characterize them as damped oscillations with maximum frequency of about 3 Hz with damping rate of about 0.27 Hz/min. Wavelet coherency analysis reveal that high-frequency  $\text{Ca}^{2+}$  oscillators can interfere with the third and second harmonics of sinus rhythm, leading to the presence of time intervals with increased coherence between the aberrant and normal rhythm. These data imply that in failing cardiomyocyte can be autonomous self-regulation mechanism of reducing frequency and normalization. The findings suggest possible involvement of abnormal  $\text{Ca}^{2+}$  release from the sarcoplasmic reticulum in the process of arrhythmogenic activity of the heart in hypoxic condition.

**Key words:** calcium waves, cardiomyocytes, myocardium, ischemia, arrhythmia, wavelet coherence

## INTRODUCTION

Integral  $\text{Ca}^{2+}$  release from the sarcoplasmic reticulum following action potentials propagating along the excitable membrane of cardiomyocytes is the main factor initiating a contractile response. Arrhythmias associated with myocardial damage are one of the leading causes of death in the ageing human population ((1)). An intracellular accumulation of  $\text{Ca}^{2+}$  caused by a failure of the ATP-dependent mechanisms known to be the key events in myocardial damage during ischemia (2–4). In the process of damage progression functional myocardial tissue becomes  $\text{Ca}^{2+}$ -overloaded and then lost functionality with the properties of  $\text{Ca}^{2+}$  waves changing progressively over time (5, 6). Under a number of adverse conditions and/or according to individual heart diseases, abnormal forms of  $\text{Ca}^{2+}$  release from the sarcoplasmic reticulum are observed, which may cause arrhythmogenesis (7). One form of this abnormal release is spontaneous space-time changes in the level of  $\text{Ca}^{2+}$  in the cytoplasm (sporadic  $\text{Ca}^{2+}$  waves), observed both in isolated cardiomyocytes (2, 3) and in situ experiments, including the perfused heart (4, 5). However, the sources of these waves, the conditions for their appearance, as well as their role and influence on the heart muscle, are not well understood. It is known that hypoxia of the heart muscle is often accompanied by tachycardia, group extrasystoles, bouts of paroxysmal rhythm disturbances. The extent to which these violations can be associated with the appearance of  $\text{Ca}^{2+}$  waves

remains unknown.  $\text{Ca}^{2+}$  dynamics at the border zones between the infarcted and non-infarcted myocardium is considered to be a key element for arrhythmogenesis (8). The aim of the work was to find out whether hypoxia as one of the factors of myocardial damage can trigger sporadic  $\text{Ca}^{2+}$  waves, and if so, can these waves affect the oscillatory activity of intact cardiomyocytes in the working heart. We applied the method of confocal microscopy and carried out a frequency analysis of calcium oscillations in cardiomyocytes from border zone between the necrotic and healthy myocardium. So far, wavelet transformation has been used only for feature extraction in the analysis of hyperspectral laser-induced fluorescence data ((9)) and for the analysis of electrocardiogram ECG-derived data ((10)). In this paper, we demonstrate the capabilities of wavelet transform for the analysis of in situ confocal microscopy-derived fluorescence data from isolated working heart.

## MATERIALS AND METHODS

Capitalize trade names and give manufacturers full names and addresses (city and state).

### Animals

Studies were conducted in accordance with regulations of the National Committee on Bioethics of the Russian Academy of Sciences. The protocol was approved by the Ethics Committee of the Sechenov Institute of Physiology and Evolutionary Biochemistry. Experiments were performed in hearts isolated from adult Wistar male rats ( $N = 10$ ; body weight 200–250 g).

### Heart staining

Animals were anesthetized with sodium Nembutal (50 kg - 1 , i.p., 50 mg), and then the hearts were harvested/removed via thoracotomy. The model of an isolated perfused working rat heart was method of Langendorff. The preparation was retrogradely perfused via the aortic cannula through with a Tyrode's solution of the following composition (mM): 140 NaCl, 1.0  $\text{MgCl}_2$ , 4.5 KCl, 10 glucose, 1  $\text{CaCl}_2$  and 10 HEPES. The pH of the solution was maintained at 7.4 by continuously bubbling with 95%  $\text{O}_2$ /5%  $\text{CO}_2$  and temperature maintained at 37  $^{\circ}\text{C}$ . Effluent was drained via a catheter placed in dish so as not to touch the heart. Myosin ATPase inhibitor, blebbistatin (10  $\mu\text{M}$ , Sigma, USA) was added to the Tyrode's solution perfusing the heart to stop heart contraction and prevent associated artifacts (Farman et al., 2008). To prevent motion artifact in optical recordings, muscle contraction was inhibited with 20  $\mu\text{M/L}$  of (-)-blebbistatin (11). The dyes Fluo-4-AM, Tetramethylrhodamine Methyl Ester Perchlorate, TMRM, and Di-8-ANEPPS, was obtained from Thermo Fisher Scientific. Heart perfusion was performed using a modified Langendorff system. Tyrode solution with  $\text{CaCl}_2$  (1 mM/L) was used as the perfusion medium. A similar solution with the addition of the fluorescent dyes Fluo-4 (20  $\mu\text{M/L}$ ) and Di-8-ANEPPS (20  $\mu\text{M/L}$ ) was used for visualization of the  $\text{Ca}^{2+}$  waves. For dyeing mitochondria, the TMRM dye was used, the fluorescence intensity of which is proportional to the value of the mitochondrial membrane potential ( $\Delta\psi$ ). For simultaneous visualization of free  $\text{Ca}^{2+}$  ions and membrane potential in cardiomyocytes, the Fluo-4 dye was used in combination with Di-8-ANEPPS. Perfusion of the hearts was performed with combinations of solution: Fluo-4 and TMRM, Fluo-4 and Di-8-ANEPPS.

### Confocal microscopy

The subepicardial layers of the myocardium were examined using an inverted Leica TCS SP5 laser scanning confocal microscope equipped with a resonance scanner and with a x10, x20, x63 oil immersion lenses (Leica, Germany). To investigate fluorescent signals in myocardium, we positioned isolated perfused heart in organ bath with thin bottom (180  $\mu\text{m}$ ), left ventricle was in conjunction with an oil-immersible objective lens on an inverted microscope. This setting provide sufficient depth discrimination to focus directly onto the epicardial layers and individual cells within the intact functioning organ. With the simultaneous detection of fluorescence Fluo-4 and Di-8-ANEPPS, an argon laser with a wavelength of 488 nm and a power of 80% was used to excite the fluorescence. To the simultaneous detection of fluorescence of Fluo-4 and TMRM we used an argon laser with a wavelength 488 nm and a power of 80% and a HeNe laser with a wavelength of 543 nm and a power of 80%. Fluorescence detection was carried out using two photomultiplier tubes (PMT) in the spectral range 493—540 nm for Fluo-4 and 552—792 nm for TMRM. The pinhole was set to 200 mm, resulting in , 2.5- $\mu\text{m}$  optical slices. Amplifier gain and detector offset were adjusted such that neither saturation nor threshold cutoff occurred. Since the specific values of the background fluorescence depended on the density of the capillary network, the amount of connective tissue in the field of view, and other factors, the sensitivity of the PMT detector (gain) was selected individually each time, depending on the conditions of the survey, and was usually 600 to 800 units. Changes in fluorescence intensity of all used dyes over time ( $xyt$  mode) were measured with a resonant scanner (8000 Hz), while the diameter of the confocal pinhole was set to 100  $\mu\text{m}$ . The fluorescent signal was measured in a whole frame or in certain regions of interest (regions of interest, ROI).

## Data collection and analysis

Recorded time-series image stack were analyzed in ImageJ v.1.52p software (12). Area = 318.363, x = 17.8427296118,  $\approx$  17.84  $\mu\text{m}$ . Scaling: 455.9  $\mu\text{m}$  in 512px, 1 px = 0.8904296875  $\mu\text{m}$ . 576 ROI 17.84 x 17.84  $\mu\text{m}$  were selected using ImageJ macros (see Supplementary). Time series were obtained in BAR plugin using multi ROI profiler from image stack with as raw signals and after normalization against F0 and saved as csv files. The accumulation, correction, systematization of the initial information were carried out in Microsoft Office Excel 2016 spreadsheets. Visualization of the obtained results and Time series analysis was done using the free software computing environment R v. 3.5.3 ((13)).

Frequency estimation was done using Fast Fourier Transform with Kaiser or Hamming window with dynamic range adjusting 40 to 65 in depend on signal amplitude — available as spectrogram function in phonTools package. Spectral analysis of calcium oscillations was carried out using a fast Fourier transform. We decided to apply a wavelet analysis of calcium oscillation frequencies (14). The transform provides information on both local amplitude and instantaneous phase of any periodic process across time with subsequent investigation of coherency between two time series ((15), (16)). Wavelet analysis was performed with package WaveletComp ((17)). WaveletComp (version 1.1) analyzes the frequency structure of uni- and bivariate time series using the Morlet wavelet.

The “mother” Morlet wavelet is:

$$\psi(t) = \pi^{-1/4} e^{i\omega t - t^2/2} \quad (1)$$

In formula 1 “angular frequency”  $\omega$  is set to 6 since it makes the Morlet wavelet approximately analytic. The Morlet wavelet transform of a time series ( $x_t$ ) is defined as the convolution of the series with a set of “wavelet daughters” generated by the mother wavelet by translation in time by  $\tau$  and scaling by  $s$ :

$$\text{Wave}(\tau, s) = \sum_t x_t \frac{1}{\sqrt{s}} \psi^* \left( \frac{t - \tau}{s} \right) \quad (2)$$

In formula 2  $\tau$  is the localizing time parameter defines position of the particular daughter wavelet in the time domain, and the set of scales  $s$  determines the wavelet coverage of the series in the frequency domain. WaveletComp uses Fast Fourier Transform algorithms to evaluate formula 2 efficiently. The evolving in time local amplitude of any periodic component of the time series can then be retrieved from the modulus of its wavelet transform with rectification:

$$\text{Ampl}(\tau, s) = \frac{|\text{Wave}(\tau, s)|}{\sqrt{s}}. \quad (3)$$

The wavelet power spectrum is the square of the amplitude, understand as time-frequency (or time-period) wavelet energy density:

$$\text{Power}(\tau, s) = \frac{|\text{Wave}(\tau, s)|^2}{s}. \quad (4)$$

Displacements of periodic phenomena relative to the localizing origin  $\tau$ , shifted across the time domain, are given by the instantaneous or local wavelet phase. It can be wrapped to represent an angle in the interval  $[-\pi, \pi]$ :

$$\text{Phase}(\tau, s) = \text{Arg}(\text{Wave}(\tau, s)) = \tan^{-1} \left( \frac{\text{Im}(\text{Wave}(\tau, s))}{\text{Re}(\text{Wave}(\tau, s))} \right). \quad (5)$$

The concepts of cross-wavelet analysis provide appropriate tools for (i) comparing the frequency contents of two time series, (ii) drawing conclusions about the series’ synchronicity at certain periods and across certain ranges of time. The cross-wavelet transform of two time series (x t) and (y t), with respective wavelet transforms Wave.x and Wave.y, decomposes the Fourier co- and quadrature-spectra in the time-frequency (or time-scale) domain. WaveletComp implements the rectified version according to Veleda et al. [16]:

$$\text{Wave.xy}(\tau, s) = \frac{\text{Wave.x}(\tau, s) \cdot \text{Wave.y}^*(\tau, s)}{s} \quad (6)$$

Its modulus can be interpreted as cross-wavelet power; it lends itself, with certain limitations, to an assessment of the similarity of the two series’ wavelet power in the time-frequency (or time-scale) domain:

$$\text{Power.xy}(\tau, s) = |\text{Wave.xy}(\tau, s)| \quad (7)$$

Information about the two series’ synchronization in terms of the instantaneous or local phase advance of any periodic component of (x t) with respect to the correspondent component of (y t), viz. the so-called phase difference of x over y at each localizing time origin and scale:

$$\text{Angle.xy}(\tau, s) = \text{Arg}(\text{Wave.xy}(\tau, s)) \quad (8)$$

This equals the difference of individual phases, Phase.x — Phase.y, when converted to an angle in the interval  $[-\pi, \pi]$ . Phase differences are displayed as arrows in the image plot of cross-wavelet power. In order to analyze displacements of periodic phenomena in two time series, a comparative plot of wavelet coherency may be helpful. Wavelet coherency measures the cross-correlation between two time series as a function of frequency: the wavelet coherence is given by the formula:

$$\text{Coherence} = \frac{|s\text{Wave.xy}|^2}{s\text{Power.x} \cdot s\text{Power.y}} \quad (9)$$

The need for smoothing is indicated by the prefix s.

Wavelet coherence images of two time series provided by correspondent ROI fluorescent imaging within subepicardial layer. The vertical axis shows the Fourier periods. The horizontal axis shows time step counts. Contour lines added to the wavelet power spectrum delineate areas of high significance. Wavelet power spectrum of the series with variable period. Horizontal arrows pointing to the right indicate that the two series x and y are in phase at the respective period with vanishing phase differences. Likewise, horizontal arrows pointing to the left indicate that the two series are in anti-phase; The arrows are plotted only within white contour lines indicating significance (with respect to the null hypothesis of white noise processes) at the 10% level. 10 simulations using analyze.wavelet function from WaveletComp package was run do plot Cross-Wavelet power spectrum of the series with interval color key and restricted arrow area. Limit the area where arrows are drawn to the region where both individual wavelet transforms of x and y show significance (set which.arrow.sig = "wt"), and avoid the artifacts. The significance level of contour lines defined to . The plot of the ridge can be restricted to a high-level region ("high" according to a given level of plotted values). In particular, the area to be filled with arrows can be determined in several ways: to reflect significance (at a given level) with respect to cross-wavelet power, wavelet coherence, or individual wavelet power, and/or to flag a high-value region. Furthermore, there is an option to clear out the area where the p-values of cross-wavelet power (coherence, respectively) exceed a given level. 30 simulations was run to compute wavelet coherency.

Calibration with a sine wave signal. 1 Hz and 3 Hz waves are represented in the picture 9. A test signal containing three sequential sinusoids.

For cluster analysis we used the PAM algorithm ((18); (19)).

## RESULTS

At the first stage of the study, we analyzed the fluorescence patterns of the heart stained for mitochondria and calcium. A fluorescent signal was registered in the first layer of cardiomyocytes adjacent to the epicardial surface of an isolated heart (Fig. 1). The (1 A, B) shows images obtained from a normal and ischemic organ. When the mitochondria and free  $\text{Ca}^{2+}$  ions were stained in the absence of contractile activity and sinus rhythm (inhibition by BDM) in the heart, they were detected as areas of the normal myocardium, characterized by a high  $\Delta \psi$  and a low value of  $\text{Ca}^{2+}$ , and areas of the myocardium, which is in different stages of ischemic damage. Different types of myocardial damage occur as more and more cardiomyocytes die. groups of cells with reduced mitochondrial potential and elevated calcium content. First, these are single dying cells, groups of cells with necrotic striation. Using an optical cut through curve region we can show connective tissue and couple of  $\text{Ca}$ -overloaded cells in an ensemble of epicardial cardiomyocytes with a normal concentration of calcium visualized with Fluo-4 (1, A). Based on a series of optical sections, a three-dimensional image of a portion of the myocardium of an isolated rat heart stained with a potential dependent Di-8-ANEPPS dye. For further observations, we will use optical sections parallel to the epicardial plane, such as the one shown in (1 D).

Calcium waves in rat myocardium against a background of global calcium release shown in figure 2. Optical sections of the epicardial region of the ventricular myocardium of the isolated working heart of the rat, painted with Di-8-ANEPPS (red) and Fluo-4 (green). B - Plots of fluorescence intensity of Fluo-4 versus time. Presented frames are indicated by black arrows. The scale segment is  $100 \mu\text{m}$ .

Optical section of the myocardium stained with Fluo-4 (green). For comparison, 12 ROIs with a size of  $10 \mu\text{m} \times 20 \mu\text{m}$  are selected. The asterisk marks areas with necrotic striation. The scale segment is  $10 \mu\text{m}$ .

Measurement duration = 109.6 s, sampling frequency = 14.142211 Hz. Since the sampling rate is 14.142211, the Nyquist frequency is 7.071105.

Studies were made of the frequency characteristics of calcium waves arising in cardiomyocytes of the border zone. For comparison, 12 cells were selected located next to the necrosis zone (Fig. 9). In each cell, an ROI was determined in which fluorescence fluctuation values of Fluo-4 were measured. The obtained values were processed by the FFT method in the Origin program, some of the frequency characteristics of the calcium waves are shown in Fig. 10 (the data table is presented in the file Fluo-4).

Comparison of calcium waves of cardiomyocytes located in the perinekrothic zone of the ventricular myocardial epicardial region of an isolated working rat heart. Plots of fluorescence intensity of Fluo-4 versus time are shown, which are typical for

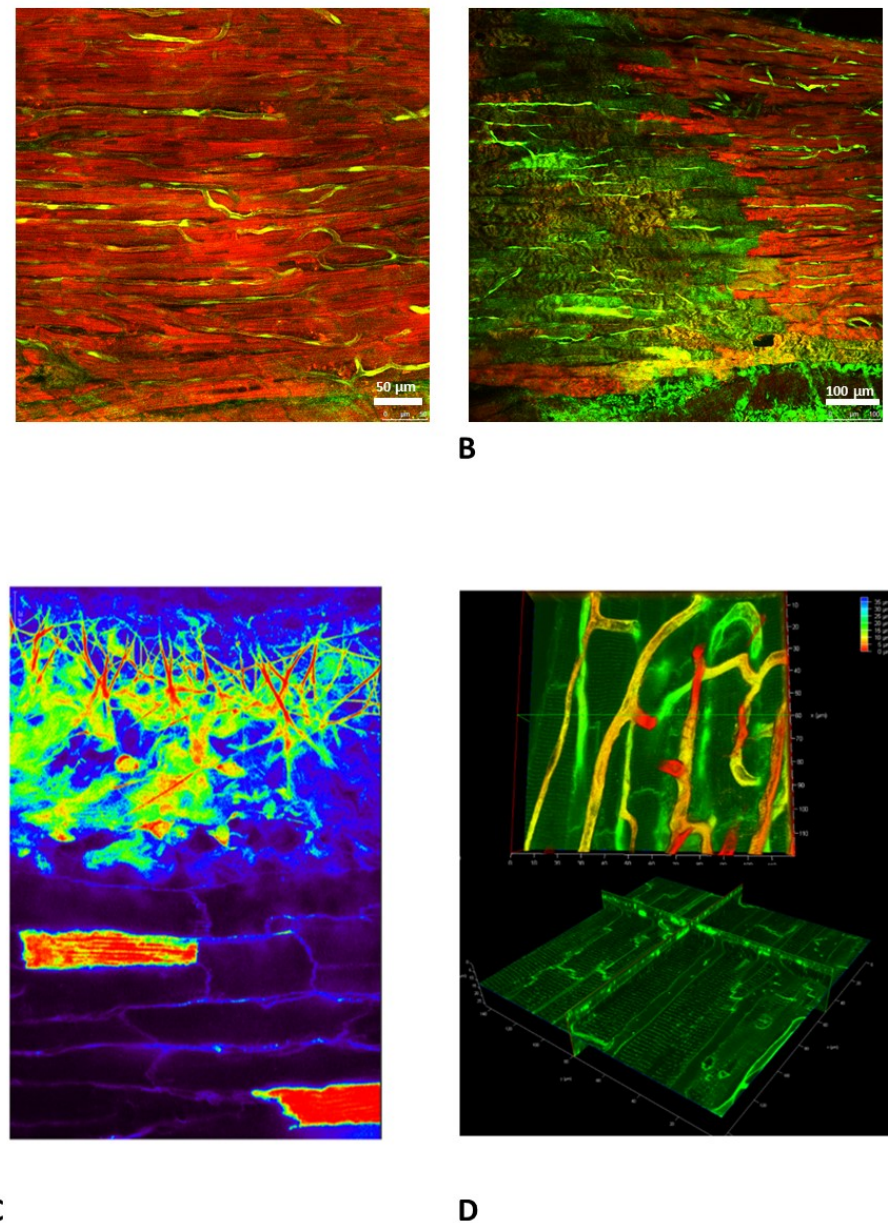


Figure 1: Confocal view in 10x objective of mitochondrial potential (red) and calcium (green) staining of epecardial cardiomyocytes in normal (A) and hypoxic (B) conditions. (C) Pseudocolor intensity imaging of Ca-overloaded cells and connective tissue in tangential section of live hear wall. (D) 3D models of cappillaries and characteristic section depth for calcium waves registration.

cells located at different stages of damage. The green line is a cell with a normal rhythm; blue line - a cell with a high content of  $\text{Ca}^{2+}$  and sinus rhythm disturbances; red line - high-frequency spindle-shaped oscillations; turquoise line - damped oscillations, cell in terminal stage; the black line is a cell in the stage of hypercontraction. Calcium waves in cardiomyocytes lying near the necrosis zone. Optical section of the myocardium stained with Fluo-4 (green) and Di-8-ANEPPS (red).

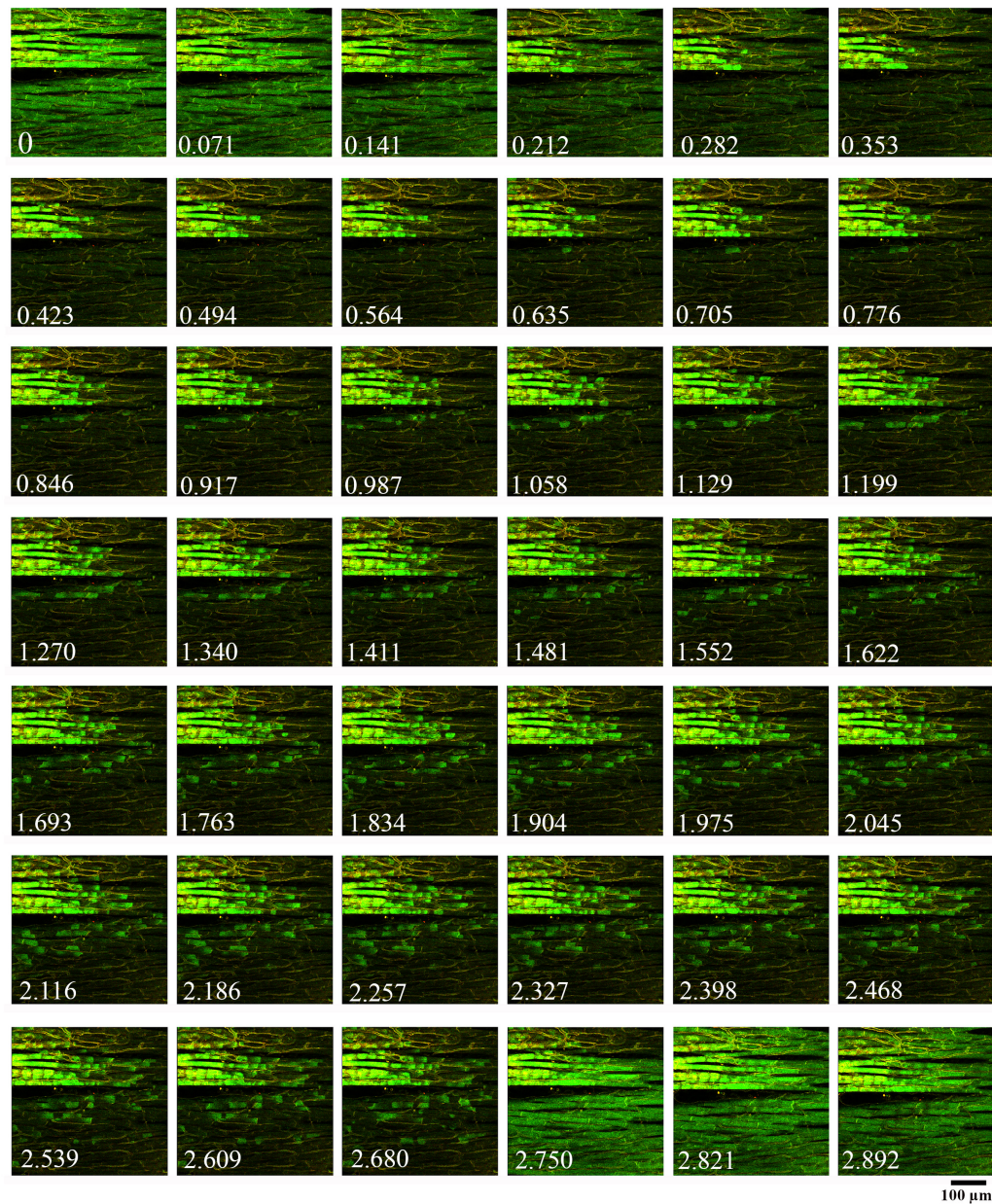


Figure 2: Frame-by-frame scanning of optical images of the epicardial layer from right ventricular myocardium of an isolated working rat heart 20 min after the onset of hypoxia.

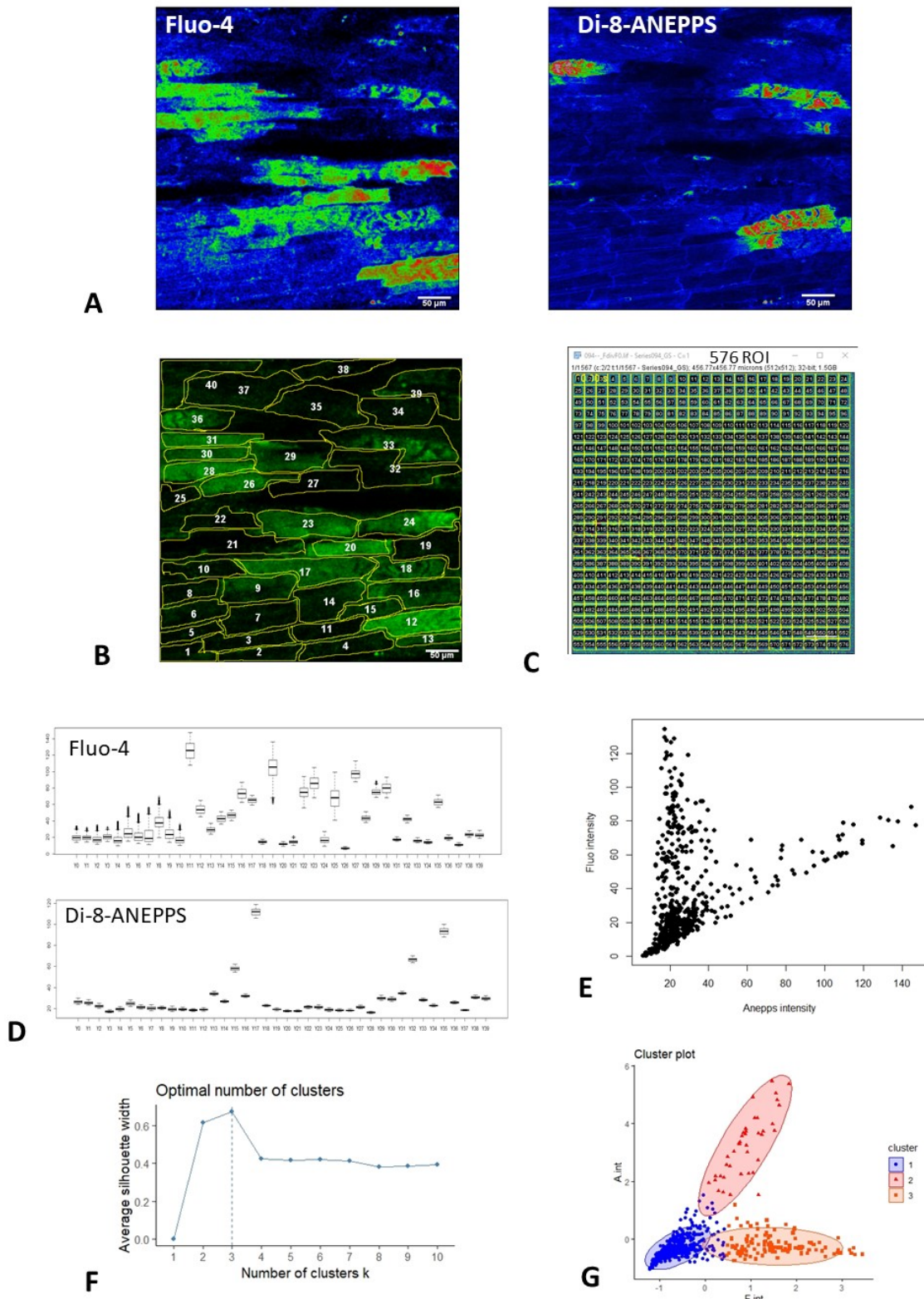
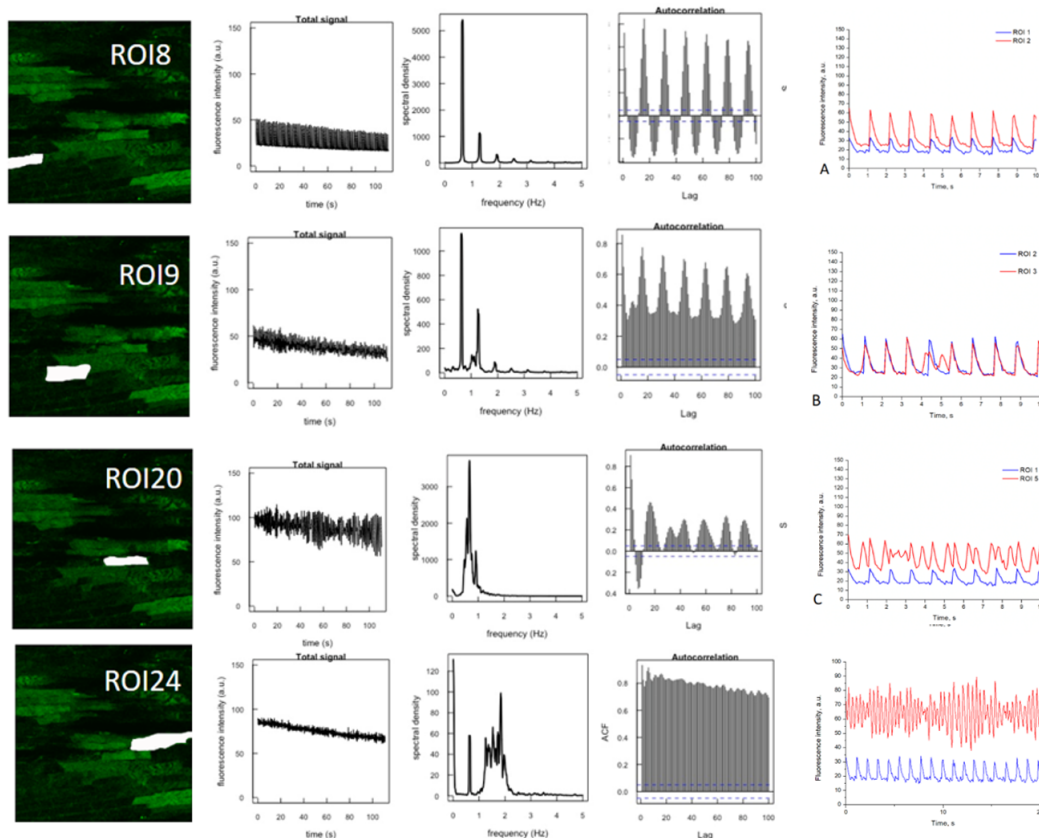


Figure 3: (A) Fluo-4 and 8-Di-ANEPPS raw signals images in spectral view. (B) Fluo-4 raw signal image in normal view with manually selected cardiomyocytes. (C) Fluo-4 raw signal image in normal view with 576 ROI grid. (D) Boxplots of Fluo-4 and 8-Di-ANEPPS raw signal intensities in 40 manually selected cells. (E) Fluo-4 and 8-Di-ANEPPS raw signals intensities plotted against each other. (F) Optimal number of clusters estimation. (G) 3 cluster partitioning visualization.



**Figure 4:** Comparison of signals from different cell ROIs: 1st column — Optical images of Fluo-4 raw signals from the epicardial layer of right ventricular myocardium of an isolated working rat heart 20 min after the onset of hypoxia. Selected ROIs are white regions. 2nd column — Total 110 sec signals in time-intensiy domain. 3d column — FFT-derived spectral density. 4th column — Autocorrelation lag plots. 5th column — Signal segments of correspondent ROIs (red) in comparison with "normal" ROI (blue line).

On the combined image, the dotted rectangles indicate the selected ROI. The scale segment is 100  $\mu\text{m}$ . On the fluorescence intensity curves of Fluo-4 in the selected ROI, damped oscillations are seen. Total observation time is 110 sec. Optical recording of sinus rhythm in the myocardium.

A - Optical sections of the epicardial region of the ventricular myocardium of the isolated working heart of the rat, painted with Di-8-ANEPPS (red) and Fluo-4 (green). B - Fluorescence intensity curves Fluo-4 (black line) and myocardial contractions (red line) versus time. Presented frames are indicated by black arrows. The scale segment is 100  $\mu\text{m}$ .

With a slight increase in the intracellular calcium concentration, such waves are erased by each subsequent global calcium release (Figure 11, B), and with a strong increase in  $\text{Ca}^{2+}$  in cardiomyocytes relative to the baseline observed in the normal myocardium, the global calcium release does not interfere with the formation of calcium waves (Fig. 11, B, D). The cardiomyocytes adjacent to the necrosis zone were characterized mainly by slow, damped calcium waves with a large amplitude (Fig. 8).

For the initial stage of damage, groups of cardiomyocytes with an elevated value of  $\text{Ca}^{2+}$ , in which high-frequency calcium waves were observed (Fig. 6), are characteristic. Nascent on the edge of the cell or in its middle, these waves can spread to neighboring cells (Figure 7). With a slight increase in the intracellular calcium concentration, such waves are erased by each subsequent global calcium release (Figure 11, B), and with a strong increase in  $\text{Ca}^{2+}$  in cardiomyocytes relative to the baseline observed in the normal myocardium, the global calcium release does not interfere with the formation of calcium waves (Fig. 11, B, D). Undoubtedly, the prognostic significance can be the detection of the switching point from the state of the cell, in which global waves can crush pathological, contributing to the restoration of a normal rhythm, to a transition through the "point of no return" when recovery is no longer possible. We found that cardiomyocytes located in the border zone adjacent to the necrosis zone are characterized by an increased content of  $\text{Ca}^{2+}$  ions, a reduced mitochondrial potential and contractile activity. Studies were made of the frequency characteristics of calcium waves arising in cardiomyocytes of the border zone. For comparison, 12 cells were selected located next to the necrosis zone (Fig. 9). In each cell, an ROI was determined in which fluorescence fluctuation values of Fluo-4 were measured. The obtained values were processed by the FFT method in the Origin program, some frequency characteristics of the calcium waves are shown in Fig. 10 (the data table is presented in the file Fluo-4 ROI 01-12.xlsx). The FFT analysis of calcium oscillations showed that in the cardiomyocytes of the perinecrosis boundary zone, as the concentration of  $\text{Ca}^{2+}$  increases, the amplitude of normal fluctuations in the concentration of ionized  $\text{Ca}^{2+}$  first increases (Figure 11, A), then single calcium waves break the sinus rhythm (Figure 11, B), then autonomous high-frequency calcium oscillations arise which, attaining a certain threshold, decay (Figure 11 B, D, Figure 12, Figure 13), after which the cardiomyocytes begin to hyper-shrink. Such calcium waves can be a source of arrhythmias and contribute to the development of contractile dysfunction in heart diseases. The cardiomyocytes adjacent to the necrosis zone were characterized mainly by slow, damped calcium waves with a large amplitude (Fig. 8).

Fig. 2. Calcium waves in rat myocardium against a background of global calcium release. Optical section of the epicardial region of the ventricular myocardium of the isolated working heart of the rat, painted Di-8-ANEPPS (red) and Fluo-4 (green), combined image. The scale segment is 100  $\mu\text{m}$ . White squares indicate the selected ROI size of 100  $\mu\text{m} \times 100 \mu\text{m}$ . Fluorescent fluorescence intensity plots in selected ROI: red line - ROI 01, green line - ROI 02. Measurement of the fluorescence intensity versus time in the myocardium, stained for active mitochondria (red) and free calcium ions (green). The scale segment is 20  $\mu\text{m}$ . Shooting for 25 min, the frame corresponding to a point of 500 seconds is presented. A plot of the fluorescence intensity measured in the frame is plotted against time.

A test signal containing 3 sequential sinusoids. Fig. 11. Pairwise comparison of calcium waves of cardiomyocytes located in

Table 1: ROI selection from 512x512 px image

	Item	Quantity	Square, $\mu\text{m}^2$
40 cells <sup>b</sup>	Cells	40	$3688.578 \pm 1567.027^{\text{a}}$
24x24 grid	ROIs	576	318.2656

<sup>a</sup> Mean ROI area and SD.

<sup>b</sup> Manually selected.

Table 2: Main peaks frequencies from 512x512 ROI

	Frequency	Amplitude
1st harmonic	0.9025	3.2154
2nd harmonic	1.7960	1.4527
3d harmonic	2.6984	0.5887

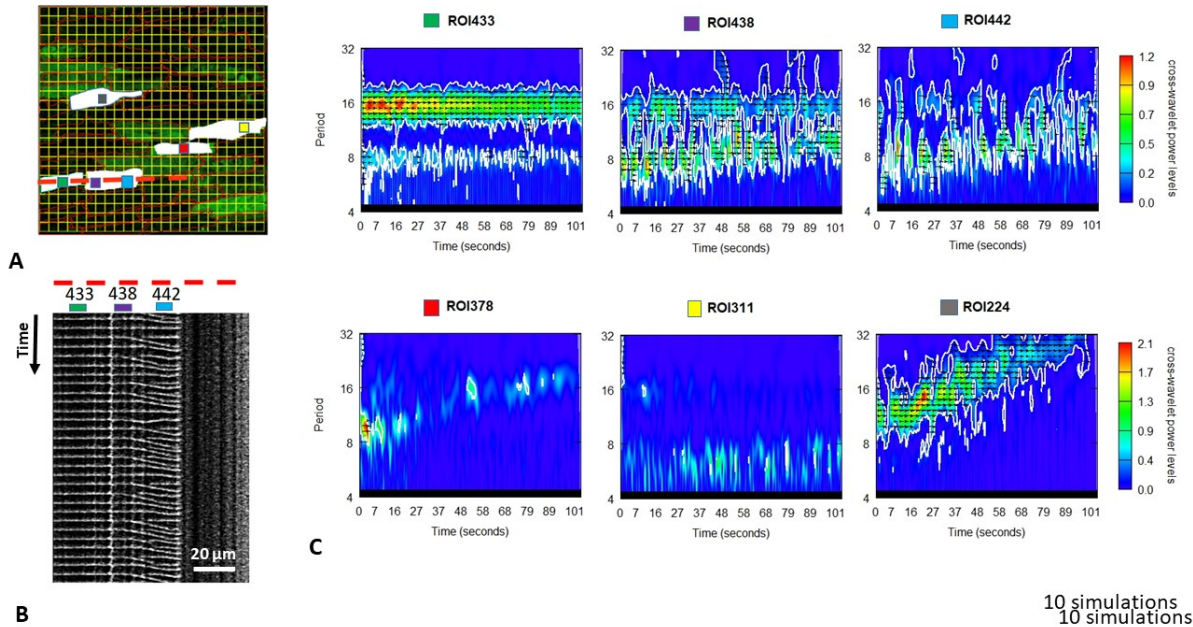


Figure 5: (A) Image (B) Kymogram (C) Cross-wavelet coherence between Fluo-4 and 8-Di-Anepps signals in selected ROIs. Power spectrum plots.

the perinekrozie zone of the epicardial region of the ventricular myocardium of an isolated working rat heart. Fluorescence intensity curves of Fluo-4 versus time are presented. A, B - comparison of signals in neighboring cells, C - comparison of signals in cells lying at a distance of 100  $\mu$ m from each other, D - comparison of signals in cells lying at a distance of 300  $\mu$ m from each other.

The FFT analysis of calcium oscillations showed that in the cardiomyocytes of the perinecrosis boundary zone, as the concentration of  $\text{Ca}^{2+}$  increases, the amplitude of normal fluctuations in the concentration of ionized  $\text{Ca}^{2+}$  first increases (Figure 11, A), then single calcium waves break the sinus rhythm (Figure 11, B), then autonomous high-frequency calcium oscillations arise that attenuate, reaching a certain threshold, (Figure 11, Figure 13, Figure 13), after which the cardiomyocytes begin to hyper-shrink. Such calcium waves can be a source of arrhythmias and contribute to the development of contractile dysfunction in heart diseases.

In the course of myocardial observations after simultaneous staining of Di-8-ANEPPS and Fluo-4 under conditions where cardiac contractions were inhibited by blebbistatin, normal myocardial regions characterized by passage of a global calcium-ejection wave corresponding to sinus rhythm and small contractions were revealed. Tissue abbreviations were determined by averaging the Di-8-ANEPPS fluorescent signal from ten arbitrarily selected ROIs of 20  $\mu\text{m} \times 20 \mu\text{m}$  size (Figure 5). Also, the areas of the myocardium, located in different stages of ischemic damage, were identified. For the initial stage of damage, groups of cardiomyocytes with an increased value of  $\text{Ca}^{2+}$ , in which high-frequency calcium waves were observed (Fig. 6), are characteristic. Nascent on the edge of the cell or in its middle, these waves can spread to neighboring cells (Figure 7). Pairwise comparison of the frequencies of calcium waves of cardiomyocytes located in the perinekrozie zone of the ventricular myocardial epicardial region of an isolated working rat heart. A - comparison of signals in neighboring cells, B - comparison of signals in cells lying at a distance of 200  $\mu\text{m}$  from each other

#### Simultaneous recordings of AP-induced and spontaneous calcium transients

norm coherence was used as a control in cell 9, an increase in coherence is observed as the frequency decreases to the second harmonic of sinus rhythm 16 with damped low frequency oscillations self-coherence increases in intensity and does not change in phase cell 10 is shrinking, it can be seen on non-normalized video (see appendix)

We performed a calculation of the 5 coherence between the sinus rhythm and cardiomyocytes in various stages of damage. The role of calcium in regulation of contraction. in the occurrence of arrhythmias.

Spontaneous Ca waves in cardiomyocytes is associated with local damage sites. Fig. 1 A shows a comparison of  $\text{Ca}^{2+}$  levels in normal (ROI1) and locally damaged (ROI11) cells along with maximum  $\text{Ca}^{2+}$  level registered from totally Ca-overloaded hypercontracted cell.

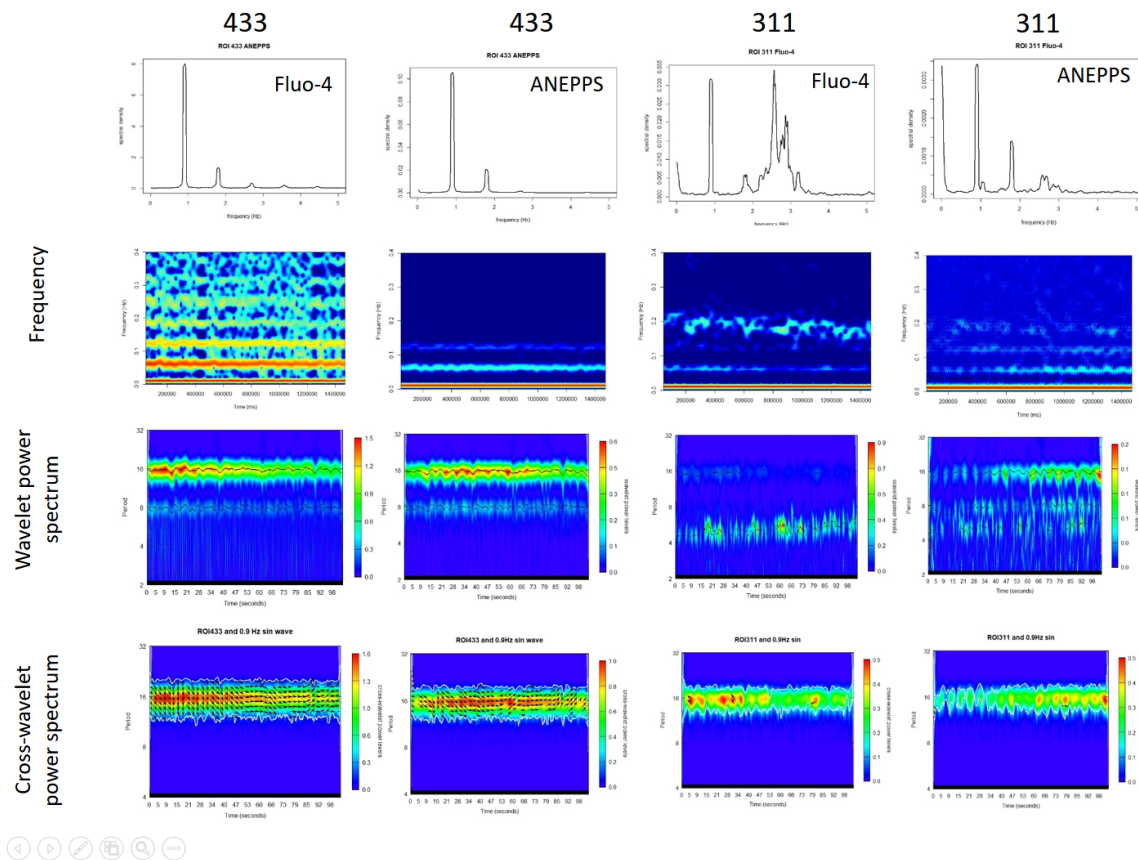


Figure 6: Analysis of selected ROIs

The scale segments are  $100 \mu\text{m}$ . Measurement of fluorescence intensity in the area of the myocardium stained for active mitochondria (red) and free calcium ions (green). The scale segment is  $50 \mu\text{m}$ . For comparison, six ROIs of  $10 \mu\text{m} \times 20 \mu\text{m}$  are selected. Pixel intensity distribution histograms were constructed for each ROI.

In the book (20) about atrial fibrillation ... Arrhythmia

**Word** Definition

**Concept** Explanation

**Idea** Text

An example quotation:

  Lorem ipsum dolor sit amet, consectetur adipiscing elit, sed do eiusmod tempor incididunt ut labore et dolore magna aliqua. Ut enim ad minim veniam, quis nostrud exercitation ullamco laboris nisi ut aliquip ex ea commodo consequat.

## DISCUSSION

To investigate spontaneous  $\text{Ca}^{2+}$  waves and sinus rhythm in myocardium, we used wavelet methodology as a reasonable choice to study periodic phenomena in time series, particularly in the presence of potential frequency changes across time.

Measurements of  $\text{Ca}^{2+}$  waves in isolated rat heart. Now it is well acknowledged that  $\text{Ca}^{2+}$  - overloaded cardiomyocytes are essential substrate for arrhythmias and contractile failure, especially in acute myocardial infarct.

We decided to use this method for the analysis of calcium oscillations in the myocardium of a working heart. The experimental limitations of the method used allowed us to register 100 seconds of the signal. We cannot register a signal

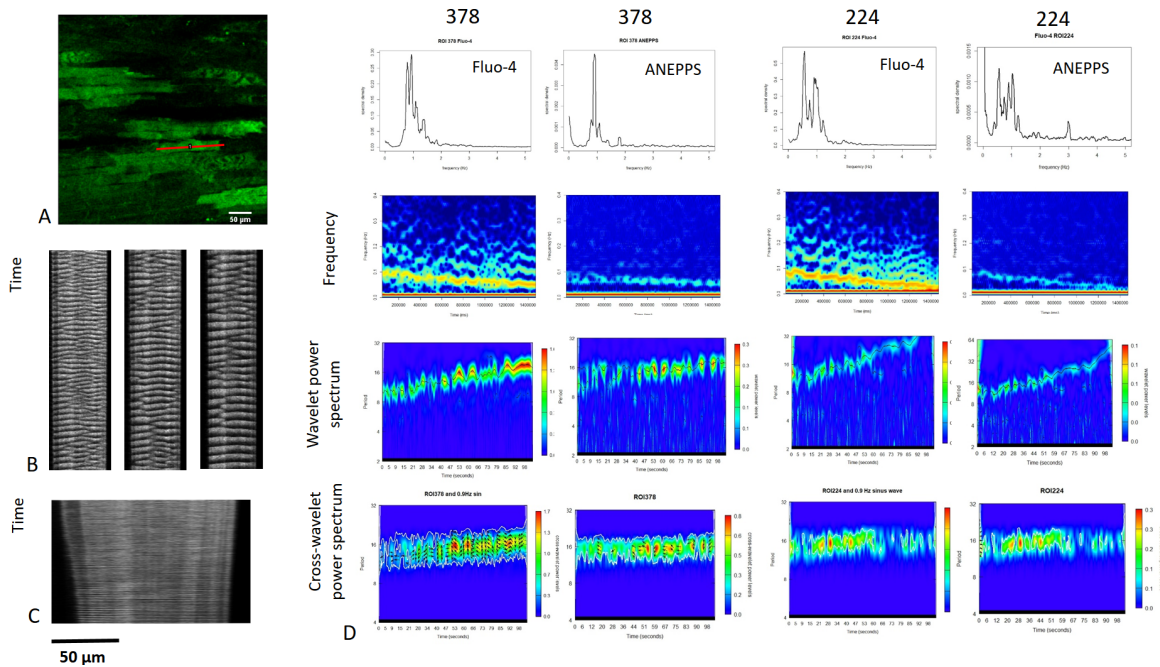


Figure 7: (A) Image (B) Kymogram (C) Kymogram (D) Analysis of selected ROIs

of sufficient duration to fully trace the evolution of frequency-amplitude characteristics in a pathological ischemic process. Therefore, we applied a comparative analysis of these characteristics recorded from cardiomyocytes at various stages of damage.

For optical registration of calcium waves we implement method described by (21). Calcium waves in the subepicardial myocardium in Langendorff-perfused rat heart. We found that cardiomyocytes located in the border zone adjacent to the necrosis zone are characterized by an increased content of  $\text{Ca}^{2+}$  ions, a reduced mitochondrial potential and contractile activity. Unstationarity in Calcium Oscillations in Isolated Heart Revealed by Wavelet Analysis. Spectral analysis of hypoxia-induced calcium waves in isolated rat heart on the subcellular level reveal local hypercontraction sites as sources for high-frequency oscillations. Wavelet transform coherence (WTC) is a method for analyzing the coherence and phase lag between two time series as a function of both time and frequency ((22)). Local hypercontracts are centers of high-frequency calcium oscillations damage progression line. (23) provide the first demonstration of local, transient  $\text{Ca}^{2+}$  entry (LoCE) events, which comprise cardiac SOCE.

As was clearly demonstrated (21), Ischemic myocardial damage manifests itself as a source of calcium waves. We show in this paper, on a model of an isolated rat heart, what the frequency characteristics of calcium oscillations recorded in the border zone near necrosis. Intracellular calcium accumulation caused by weakening of ATP-dependent mechanisms due to lack of oxygen supply causes foci of high-frequency calcium oscillations that go out of control by sino-atrial rhythm.

Scale modeling approach that spans from single channel to whole-cell and spatial simulations, we show that both CICR and SOICR gating modes can indeed activate RyR2 channels and modify  $\text{Ca}^{2+}$  spark dynamics in a manner consistent with experimental observations. However, detailed comparison of  $\text{Ca}^{2+}$  wave generation and CRU-to-CRU  $\text{Ca}^{2+}$  wave propagation shows that CICR alone is a sufficient, and necessary, mechanism to explain  $\text{Ca}^{2+}$  release in heart under both physiological and pathological conditions (24).

In the ischemic myocardium  $\text{Ca}^{2+}$  waves are regarded as arrhythmogenic substrates. To quantitatively image how  $\text{Ca}^{2+}$  waves interfere with  $\text{Ca}^{2+}$  transients from spontaneous sinus rhythm we used a single-photon confocal laser scanning microscopy in Langendorff-perfused rat hearts. This technique has allowed Intravital imaging visualization of  $\text{Ca}^{2+}$  waves propagation at the single-cell level in epicardial cardiomyocytes, avoiding the damage induced by isolation of cardiomyocytes. The effects of hypoxia on oscillations in intracellular calcium concentration  $\text{Ca}^{2+}$  were determined in isolated rat heart. The aim was to investigate the frequency characteristics of calcium oscillations arising in the epicardium in response to ischemia. Spectral analysis of myocardial analysis of calcium oscillations in rat heart using confocal microscopy was carried out. Optical recording of calcium currents in the rat myocardium during the development of ischemic injury. In cells located at the periphery of the lesion focus, the basal level of calcium remains within normal limits, point-like, prismatic wave sources appear that do not extend to the cell as a whole and are extinguished by a wave of normal ejection. A wave of normal ejection is the result of the work of

the pacemaker cells and is accompanied by a synchronous muscle contraction. In cells closer to the lesion focus, the calcium concentration rises. Microtraumas, points of damage are sources of waves. As a result of the hyperscrubbing of ischemic cells, there are gaps between the cardiomyocytes that become the sources of individual transverse waves that cover the whole cell and are able to spread to neighboring cells. As a result of interference of several calcium waves, wave packets arise, the amplitude of which increases as the intracellular concentration of free calcium ions increases. An arrhythmia arises, representing a group of partially damaged and contiguous intact myocardial cells characterized by an elevated concentration of free calcium ions that have their own rhythms of calcium release and muscle contractions and are not affected by pacemaker cells. and during the detachment of the cell the frequency increases spasmodically. Intracellular calcium waves were intensively studied in isolated cardioiocytes by the linescan method (Gyorke, Sunil Kapur). The results obtained revealed the large role of calcium sparks in the nucleation of these waves. Spectral analysis of measure the intensiy of Systolic  $\text{Ca}^{2+}$  alternans hypercontracture-indused calcium oscillations interfere with Systolic  $\text{Ca}^{2+}$  alternans SR  $\text{Ca}^{2+}$  content changes during alternans (25). We assume that high-frequency calcium oscillations arise at the time of cardiomyocyte damage caused by hypercontraction. We assume that such high-frequency activity may cause arrhythmias. Since in the course of hypercontraction initial damage can be localized as two adjacent sarcomeres, Propagation of transverse calcium wave along longitudinal axis Such anisotropic protagation of calcium waves was described in 1994 by Engel et al, and velocity of wave propagation rise with temperature. Formation of calcium waves of different type in isolated cardiac myocytes (26) that this type of calcium waves initiate from stochastic (27) subdiffusive (28) Chen et al calcium sparks. This propagation pattern was satisfactorily explained by Finite-element simulations of the three-dimensional cell model, conducted for different intracellular locations of triggering calcium sparks (29) we observed for 100 sec Sustained transverse calcium wave patterns in epicard of isolated heart for some time the damaged cardiomyocyte, which has not lost its connection with neighboring cells, can be a source of high-frequency calcium waves, which are transmitted to neighboring cells through gap junctions. Tomoyuki at al using confocal device with simultaneous recording of electrocardiograms demonstrated that  $\text{Ca}^{2+}$  waves in Langendorff-perfused rat hearts were completely abolished by ventricular excitation, and that under highly  $\text{Ca}^{2+}$  -overloaded conditions  $\text{Ca}^{2+}$  waves may occur more frequently and propagate more prevalently to the surrounding cells. Authors suggested that  $\text{Ca}^{2+}$  waves play little, if any, pathophysiological role (6,7). Later, it was established that myocardial injury induces  $\text{Ca}^{2+}$  waves in the heart (8,9). Baader et al proposed that spatio-temporal summation of changes in membrane potential caused by individual  $\text{Ca}^{2+}$  waves may underlie the generation of triggered electrical ectopic impulses (10). In recent years, it has become apparent that myocardial ischemia can cause ventricular arrhythmias and sudden cardiac death.

Calcium waves. How calcium waves are formed and what the consequences may be. Solitons. Coherence with its own main harmonic can be considered as an indicator of normality.

Future work is needed to understand the contributions of these mechanisms, as they may affect the conditions under which the model exhibits DADs during pacing. By using the in situ rapid confocal imaging system we found that in Langendorff-perfused rat heart has to show spatiotemporally  $\text{Ca}^{2+}$  dynamics.

According to (30), spontaneous  $\text{Ca}^{2+}$  waves during diastole are indicative of cellular  $\text{Ca}^{2+}$  overload .

In principle, individual atrial myocytes in the perfused hearts showed spatiotemporally uniform  $\text{Ca}^{2+}$  dynamics with frequency-dependent abbreviation of  $\text{Ca}^{2+}$ -transient durations, a confirmation of the atria being a functional syncytium.

However, even under apparently intact Langendorff perfusion, individual myocytes often exhibited spatially non-uniform  $\text{Ca}^{2+}$  dynamics, e.g., cluster-like rises of  $\text{Ca}^{2+}$ , wave-like propagation of  $\text{Ca}^{2+}$ , and beat-to-beat variability of durations and amplitude alternans of  $\text{Ca}^{2+}$  transients, all of which emerged on excitation instead of uniform  $\text{Ca}^{2+}$  transients ((31), (32)).

Analysis of calcium alternans in ischemic condition reveal spectrum of cell conditions that may affect cardiac function.

Spectral analysis of hypoxia-indused calcium waves in isolated rat heart on the subcellular level. Spontaneous calcium oscillations in unstimulated heart muscle. Local hypercontracture induces hight-frequency calcium oscillations. The frequency of high-frequency waves decreases over time in cells that are gradually hyper-contracted.

The decrease in the frequency of oscillations in time is shown. It is damaged cells that are in the process of over-contraction are the sources of oscillations ((33)).

Short Time Fourier Transform (STFT) analysis provides information about the number of oscillators, but its time resolution is limited.

Wavelet tranform allows analysis of non-stationary signals.

The presented results of wavelet tranform of obtained oscillation time dependencies confirmed the presence of several harmonic components in signal and allowed more accurate visualization of the frequency changes in time.

Thus, for the first time we demonstrated calcium oscillations frequency dynamics in myocardium.

## CONCLUSION

Sed ut perspiciatis unde omnis iste natus error sit voluptatem accusantium doloremque laudantium, totam rem aperiam, eaque ipsa quae ab illo inventore veritatis et quasi architecto beatae vitae dicta sunt explicabo. Understanding these mechanisms will help to further protect the heart muscle during cardiac surgery and in the long run will improve the prevention of heart disease.

## AUTHOR CONTRIBUTIONS

Author2 designed the research. Author1 carried out all simulations, analyzed the data. Author1 and Author2 wrote the article.

## FUNDING

This work was supported by the Russian Foundation for Basic Research (project no. 19-015-00139 A)

## ACKNOWLEDGMENTS

We thank B. Harper and J. Doe for their help.

## REFERENCES

1. Xiao, Y.-F., 2011. Cardiac arrhythmia and heart failure: From bench to bedside. *Journal of geriatric cardiology: JGC* 8:131.
2. Shen, A. C., and R. B. Jennings, 1972. Myocardial calcium and magnesium in acute ischemic injury. *The American journal of pathology* 67:417.
3. Shen, A. C., and R. B. Jennings, 1972. Kinetics of calcium accumulation in acute myocardial ischemic injury. *The American journal of pathology* 67:441.
4. Nayler, W. G., 1981. The role of calcium in the ischemic myocardium. *The American journal of pathology* 102:262.
5. Minamikawa, T., S. H. Cody, and D. A. Williams, 1997. In situ visualization of spontaneous calcium waves within perfused whole rat heart by confocal imaging. *American Journal of Physiology-Heart and Circulatory Physiology* 272:H236–H243.
6. Hama, T., A. Takahashi, A. Ichihara, and T. Takamatsu, 1998. Real time in situ confocal imaging of calcium wave in the perfused whole heart of the rat. *Cellular signalling* 10:331–337.
7. Ishide, N., T. Urayama, K. Inoue, T. Komaru, and T. Takishima, 1990. Propagation and collision characteristics of calcium waves in rat myocytes. *American Journal of Physiology-Heart and Circulatory Physiology* 259:H940–H950.
8. Takamatsu, T., 2008. Arrhythmogenic substrates in myocardial infarct. *Pathology international* 58:533–543.
9. Sobolev, I., and S. Babichenko, 2013. Application of the wavelet transform for feature extraction in the analysis of hyperspectral laser-induced fluorescence data. *International journal of remote sensing* 34:7218–7235.
10. Sharma, P., K. Newman, C. Long, A. Gasiewski, and F. Barnes, 2017. Use of Wavelet Transform to Detect Compensated and Decompensated Stages in the Congestive Heart Failure Patient. *Biosensors* 7:40.
11. Kong, W., and V. G. Fast, 2014. The role of dye affinity in optical measurements of  $\text{Ca}^{2+}$  transients in cardiac muscle. *American Journal of Physiology-Heart and Circulatory Physiology*.
12. Rueden, C. T., J. Schindelin, M. C. Hiner, B. E. DeZonia, A. E. Walter, E. T. Arena, and K. W. Eliceiri, 2017. ImageJ2: ImageJ for the next generation of scientific image data. *BMC bioinformatics* 18:529.
13. Team, R. C., et al., 2014. R: A language and environment for statistical computing. *R*.
14. Addison, P. S., 2018. Introduction to redundancy rules: the continuous wavelet transform comes of age.
15. Grinsted, A., J. C. Moore, and S. Jevrejeva, 2004. Application of the cross wavelet transform and wavelet coherence to geophysical time series. *Nonlinear processes in geophysics* 11:561–566.

16. Kahraman, E., and G. Ünal, 2016. Multiple wavelet coherency analysis and forecasting of metal prices. *arXiv preprint arXiv:1602.01960* .
17. Rösch, A., and H. Schmidbauer, 2016. WaveletComp 1.1: A guided tour through the R package. URL: [http://www.hsstat.com/projects/WaveletComp/WaveletComp\\_guided\\_tour.pdf](http://www.hsstat.com/projects/WaveletComp/WaveletComp_guided_tour.pdf) .
18. Kaufman, L., and P. J. Rousseeuw, 2009. Finding groups in data: an introduction to cluster analysis, volume 344. John Wiley & Sons.
19. Kassambara, A., 2017. Practical guide to cluster analysis in R: Unsupervised machine learning, volume 1. STHDA.
20. Kockskämper, J., and L. A. Blatter, 2002. Subcellular Ca<sup>2+</sup> alternans represents a novel mechanism for the generation of arrhythrogenic Ca<sup>2+</sup> waves in cat atrial myocytes. *The Journal of physiology* 545:65–79.
21. Matsuura, R., S. Miyagawa, S. Fukushima, T. Goto, A. Harada, Y. Shimozaki, K. Yamaki, S. Sanami, J. Kikuta, M. Ishii, et al., 2018. Intravital imaging with two-photon microscopy reveals cellular dynamics in the ischaemia-reperfused rat heart. *Scientific reports* 8:15991.
22. Chang, C., and G. H. Glover, 2010. Time-frequency dynamics of resting-state brain connectivity measured with fMRI. *Neuroimage* 50:81–98.
23. Bonilla, I. M., A. E. Belevych, S. Baine, A. Stepanov, L. Mezache, T. Bodnar, B. Liu, P. Volpe, S. Priori, N. Weissleder, et al., 2019. Enhancement of Cardiac Store Operated Calcium Entry (SOCE) within Novel Intercalated Disk Microdomains in Arrhythmic Disease. *Scientific Reports* 9:10179.
24. Williams, G. S., A. P. Wescott, S. E. Lehnart, and W. Lederer, 2017. How Does Calcium Overload Generate Calcium Waves in Heart? *Biophysical Journal* 112:541a.
25. Díaz, M. E., S. C. O’Neill, and D. A. Eisner, 2004. Sarcoplasmic reticulum calcium content fluctuation is the key to cardiac alternans. *Circulation research* 94:650–656.
26. Ishida, H., C. Genka, Y. Hirota, H. Nakazawa, and W. H. Barry, 1999. Formation of planar and spiral Ca<sup>2+</sup> waves in isolated cardiac myocytes. *Biophysical journal* 77:2114–2122.
27. Izu, L. T., W. G. Wier, and C. W. Balke, 2001. Evolution of cardiac calcium waves from stochastic calcium sparks. *Biophysical journal* 80:103–120.
28. Chen, W., R. Wang, B. Chen, X. Zhong, H. Kong, Y. Bai, Q. Zhou, C. Xie, J. Zhang, A. Guo, et al., 2014. The ryanodine receptor store-sensing gate controls Ca<sup>2+</sup> waves and Ca<sup>2+</sup>-triggered arrhythmias. *Nature medicine* 20:184.
29. Tracqui, P., and J. Ohayon, 2009. An integrated formulation of anisotropic force–calcium relations driving spatio-temporal contractions of cardiac myocytes. *Philosophical Transactions of the Royal Society of London A: Mathematical, Physical and Engineering Sciences* 367:4887–4905.
30. Macquaide, N., J. Dempster, and G. Smith, 2007. Measurement and modeling of Ca<sup>2+</sup> waves in isolated rabbit ventricular cardiomyocytes. *Biophysical journal* 93:2581–2595.
31. Jiang, Y., H. Tanaka, T.-a. Matsuyama, Y. Yamaoka, and T. Takamatsu, 2014. Pacing-induced non-uniform Ca<sup>2+</sup> dynamics in rat atria revealed by rapid-scanning confocal microscopy. *Acta histochemica et cytochemica* 47:59–65.
32. Aguirre, A. D., C. Vinegoni, M. Sebas, and R. Weissleder, 2014. Intravital imaging of cardiac function at the single-cell level. *Proceedings of the National Academy of Sciences* 111:11257–11262.
33. Sato, D., D. C. Bartos, K. S. Ginsburg, and D. M. Bers, 2014. Depolarization of cardiac membrane potential synchronizes calcium sparks and waves in tissue. *Biophysical journal* 107:1313–1317.

## SUPPLEMENTARY MATERIAL

An online supplement to this article can be found by visiting BJ Online at <http://www.biophysj.org>.

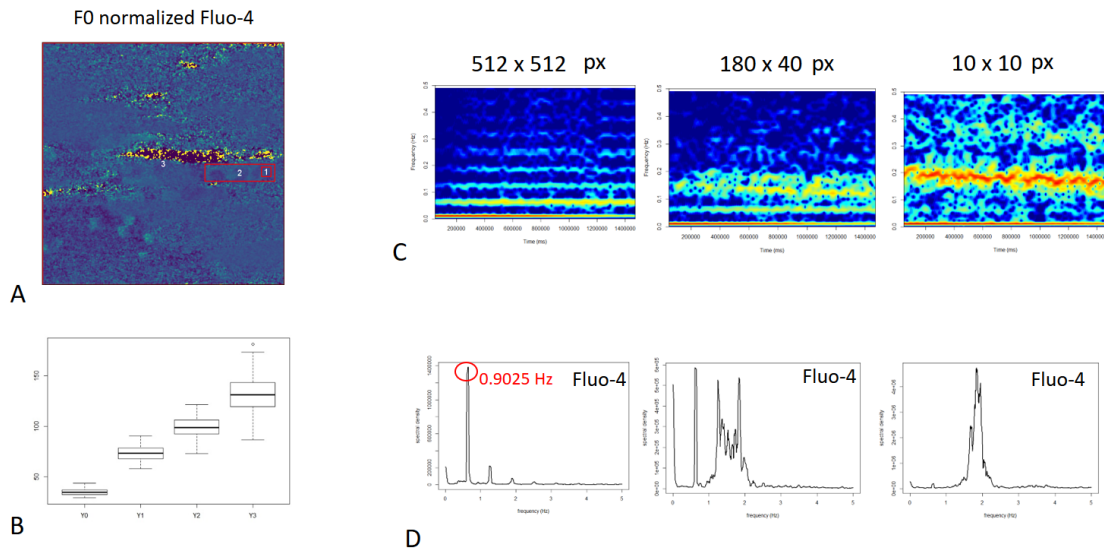


Figure 8: Comparison between signals from different size ROIs. (A) One frame from F0-normalized Fluo-4 signal, red rectangles are ROIs including damaged cell (180x40 px) and hypercontracted region of that cell (10x10 px). (B) Mean intensiy of raw Fluo-4 signal from different size ROIs: Y0 —512x512 px, Y1 — 180x40, Y2 — 10x10, Y3 — 2x2 px. (C) FFT-derived frequency spectrograms of F0-normalized Fluo-4 signals from ROIs varying in area. (D) Spectral density of F0-normalized Fluo-4 signals from ROIs varying in area. The red circle indicates peak detected as main sinus frequency

## Spatial calibration

## Frequency calibration

## Signal Clustering

ImageJ macros, R code, and raw data are available at <https://github.com/Dan609/ratheart>.

## Video files

calcium-waves-Fluo-4-ANEPPS-10fps.wmv  
094Roi.avi

## Tables in csv format

calcium.csv  
094px.csv

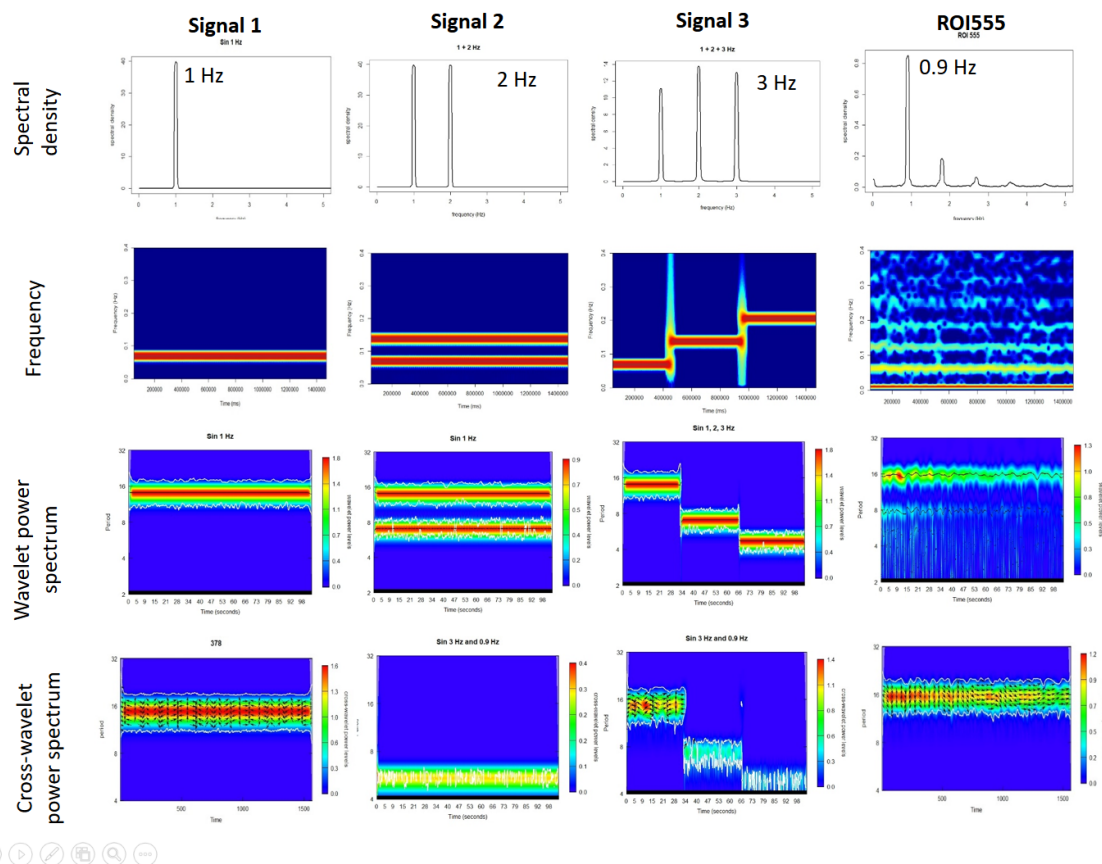


Figure 9: Comparative time series analysis of generated 1, 3 and 3 Hz sin waves with ROI555 F-0 normalized Fluo-4 signal. 1st row — Spectral density; 2nd row — FFT-derived spectrograms. 3d row — Wavelet power spectrum plots. 4th row — Cross-wavelet coherence with 0.9 Hz sin wave power spectrum plots.

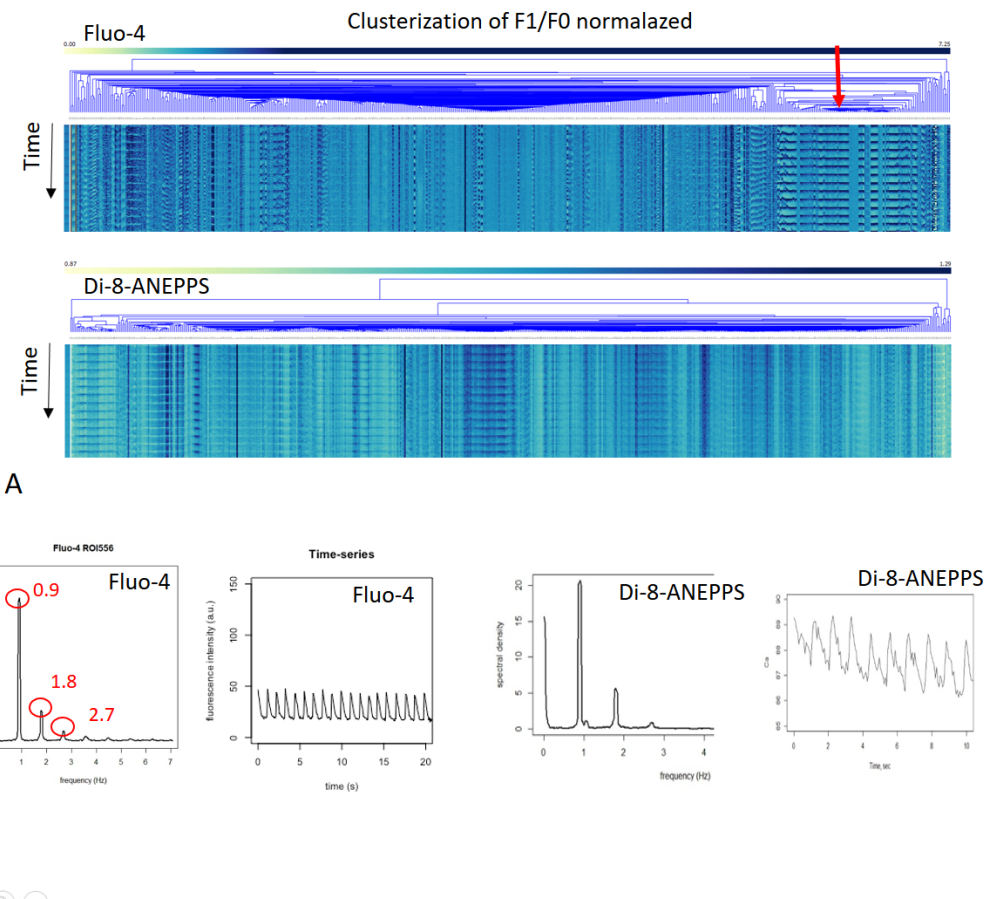


Figure 10: (A) Heat maps fragments for clusterized signals, obtained from F0-normalized Fluo-4 and 8-Di-ANEPPS signals. Red arrow indicates 'normal' ROI555. (B) Spectral density with detected peaks of F0-normalized and signal segments of raw signals.